SEMI-AUTOMATED TRACKING OF MUSCLE SATELLITE CELLS IN BRIGHTFIELD MICROSCOPY VIDEO

Ananda S. Chowdhury[1], *Angshuman Paul*[1], *Filiz Bunyak*[2], *D.D.W. Cornelison*[3], *K. Palaniappan*[2]

{aschowdhury@etce.jdvu.ac.in, angshuman.bankura@gmail.com, {bunyak, cornelisond, palaniappank}@missouri.edu}

[1]Dept. of Electronics & Telecom. Eng. Jadavpur University Kolkata-700032, India

[2]Dept. of Computer Science University of Missouri-Columbia Columbia, MO 65211, USA

[3]Division of Biological Sciences University of Missouri-Columbia Columbia, MO 65211, USA

ABSTRACT

Muscle satellite cells, also known as myogenic precursor cells, are the dedicated stem cells responsible for postnatal skeletal muscle growth, repair, and hypertrophy. Biological studies aimed at describing satellite cell activity on their host myofiber using timelapse light microscopy enable qualitative study, but high-throughput automatic tracking of satellite cells translocating on myofibers is very difficult due to their complex motion across the three-dimensional surface of myofibers and the lack of discriminating cell features. Other complicating factors include inhomogeneous illumination, fixed focal plane, low contrast, and stage motion. We propose a semi-automated approach for satellite cell tracking on myofibers consisting of registration with illumination correction, background subtraction and particle filtering. Initial experimental results show the effectiveness of the approach.

Index Terms— Satellite Cell Tracking, Particle Filters, Registration, Background Modeling

1. INTRODUCTION

Growth or repair of muscle involving the generation of new muscle cells requires the activity of a resident stem cell population, termed satellite cells [1]. Satellite cells are *activated* by extracellular cues associated with myofiber damage. Once activated, satellite cells escape out of their sublaminal niche in the membrane of the myofiber, then re-enter the cell cycle to proliferate and supply a population of committed myoblasts taking the role of muscle stem cells [2, 3]. Understanding the genetic, cellular, extracellular and biomechanical factors involved in satellite cell activation and motility is facilitated using quantitative image analysis [4]. Such studies offer the potential to improve our understanding of the processes involved in normal muscle repair, muscle aging, myopathic conditions, muscular dystrophy diseases, stem-cell based therapies and the special anticancer properties of skeletal muscle cells.

There are several challenges in the automated tracking of muscle satellite cells including complex crawling motion on the surface of the myofiber, out of focal plane cell movement, frame to frame jitter, inhomogeneous illumination and poor contrast. Fig. 1 shows myofibers with motile satellite cells in and out of the focal plane. A variety of detection-based tracking algorithms have been developed recently for the purpose of cell tracking. Ray *et al.* [5] explored a sequential Bayesian framework for automatic cell tracking. The main aim of [5] is to establish cell correspondences rather than handling of complex cell motion. Li *et al.* [6] proposed a fast active contour based 2D stem cell tracking in phase-contrast microscopy video. Nath *et al.* [7] describe a fast four-color level set based multicell tracking method. For cell tracking using graph matching, see the work of Mosig *et al.* [8], Chowdhury *et al.* [9]. Bunyak *et al.* [10] developed long-term multiple hypothesis tracking for monolayer tissues with dense nuclei.

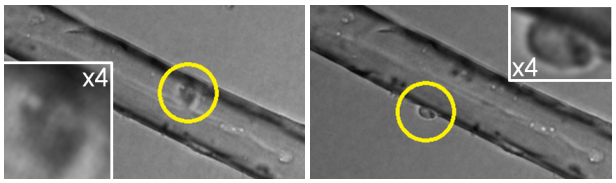

(a) (b)

Fig. 1. Muscle satellite cell moving on myofiber surface: (a) out of focal plane and occluded by the myofiber, (b) within focal plane.

To the best of our knowledge, no computer-aided methods are available to track muscle satellite cells on 3D myofibers. We propose a three-step semi-automated solution for the above tracking problem consisting of registration with illumination correction, background subtraction and particle filtering. In a supervisory mode, the proposed tracking algorithms are manually restarted when there is significant change that will likely result in errors due to: i) change of direction of a cell by more than 90° compared to the previous frame, or ii) movement of a cell out of the focal plane and occlusion by the myofiber as it crawls along the opposing surface (see Fig. 1). In the experiments the number of restarts is fixed beforehand for each cell in order to compare performance across methods. Our contribution from the perspective of image analysis lies in proposing a composite solution to a complex tracking problem. From the biomedical viewpoint, our work addresses

This work was partially supported by NIH grants AR056814 (DDWC), R33-EB00573 (KP).

the important problem of muscle stem cell tracking which has potential for high-throughput screening studies related to cell signalling, cell activation factors and muscle atrophy.

2. VIDEO PROCESSING METHODS

Our solution consists of the following three steps: a) correlation-based registration with illumination correction to stabilize the video and reduce motion artifacts arising from illumination changes; b) background modelling and subtraction to obtain an accurate foreground motion image; and c) particle filter-based tracking to estimate the position of the cells in different frames. No appearance model for the satellite cells has been explicitly used in the present work.

2.1. Registration with Illumination Correction

In this step, we take appropriate measures for handling unsteady imaging and illumination variation. Multiple fields of view per experiment were acquired by programming the microscope stage to move to specific X/Y/Z coordinates within a plate in a repetitive ten minute cycle; myofibers were imaged from the bottom. The repositioning accuracy, variation in collagen media stiffness, and subtle deformable motion of the myofiber from inertia as the stage moves, together contribute to image jitter or background (myofiber) motion. In order to remove background motion all the frames in a sequence are registered with the first frame.

However, prior to jitter compensation we first perform illumination correction based on estimating the baseline frame intensity level. Illumination changes between two frames can also result in intensity pattern differences unrelated to cell motion [11]. Let the first frame of a sequence be I_1, the k^{th} frame be I_k, and the size of each frame be $m \times n$. Then the difference image D_k associated with frame k is given by:

$$D_k(i,j) = I_k(i,j) - I_1(i,j),\ \forall (i,j), i \in [1,m], j \in [1,n] \tag{1}$$

To correct the illumination variation, we obtain the minimum of $D_k(i,j)$, denoted by D_k^{min} and subtract it from I_k. D_k^{min} ensures minimum disturbance of the floating image $I_k(i,j)$. We call this the illumination corrected image L_k,

$$L_k(i,j) = I_k(i,j) - \min_{\forall i,j}\{D_k(i,j)\} \tag{2}$$

Frame to frame jitter compensation uses a simple camera translational motion model. In order to register L_k with respect to I_1, we shift L_k by r rows, $r \in [-R, +R]$, R is the range of row shifts and c columns, $c \in [-C, +C]$, C is the range of column shifts to obtain a row-column shifted image $S_{r,c}$. We now employ normalized 2D cross-correlation, a statistically robust measure of similarity, to register $S_{r,c}$ with I_1, The normalized 2D cross-correlation, denoted by $\mathrm{NC}_{1,(r,c)}$, is given by [12]:

$$\mathrm{NC}_{1,(r,c)} = \frac{\sum_i \sum_j \left(I_1(i,j) - \bar{I_1}\right)\left(S_{r,c}(i,j) - \bar{S}_{r,c}\right)}{\sqrt{\sum_i \sum_j \left(I_1(i,j) - \bar{I_1}\right)^2}\sqrt{\sum_i \sum_j \left(S_{r,c}(i,j) - \bar{S}_{r,c}\right)^2}} \tag{3}$$

In Eq. 3, $\bar{I_1}$is the mean of I_1 and $\bar{S_k}$ is the mean of S_k. The value of r and c for which $\mathrm{NC}_{1,(r,c)}$ is a maximum (r^*, c^*) provides an estimate of row and column shift required for registration. The registered image R_k is obtained by shifting L_k by r^* rows and c^* columns. This simple method is effective to register and stabilize the sequence for background modeling.

2.2. Background Modeling and Removal

A local spatially and temporally varying median filter is used to model the background for a video frame [13]. We use a temporal window of w frames to compute the median. For the k^{th} frame of the sequence, we take the registered frames from $[k - (w-1)/2,\ k + (w-1)/2]$. Now, we compute the pixel-wise median $B_k(i,j)$ of these w registered frames to obtain the background frame B_k,

$$B_k(i,j) = \underset{p \in [(k - \frac{w-1}{2}), (k + \frac{w-1}{2})]}{\text{median}} \{R_p(i,j)\} \tag{4}$$

As the cells move, this running median produces an adaptive background model for the registered frame R_p. We obtain the foreground image F_k by subtracting B_k pixel-wise from R_k:

$$F_k(i,j) = R_k(i,j) - B_k(i,j) \tag{5}$$

Illumination correction and registration steps improve the quality of F_k. In the ideal case F_k contains only cell detections without the (myofiber) background, which can be used for particle filter based tracking.

2.3. Particle Filter-based Tracking

The motion of the cells being nonlinear, particle filter [14, 15, 16] is a justified choice to predict the position of the cells in a frame given the previous measurements. It is important to note that for the same dynamical system, the particle filter yields better accuracy compared to the extended Kalman filter when applied using a large number (∼10,000) of particles. The particle filter model equations are:

$$s_t = f_s(s_{t-1}, u_t), \quad z_t = f_z(s_t, v_t) \tag{6}$$

Here, s_t is the state vector at time instant t, f_s is the state transition function, u_t is the process noise with known distribution z_t is the measurements at time instant t, f_z is the measurement function and v_t is the measurement noise with known distribution. Eq. 6 shows both the state equation and the measurement equation [17]. We use the 2D coordinate of the cell centroid as the state vector using the ground truth for the first frame as the initial measurement. Now, if the position of the cell centroid is known at the $(k-1)^{th}$ frame, the particle filter provides a prediction for the centroid in the k^{th} frame using Eq. 6. We also need to use the measurement in frame k to guide the particle filter. Let the predicted position of the cell centroid in the k^{th} frame be (x_k, y_k). We consider a region on the order of the cell size centered at this location in image F_k. Since F_k contains primarily foreground objects

(cells), we use entropy based thresholding in this region to produce cell detections. After thresholding, connected component labeling followed by size filtering is used to extract the largest connected component. The centroid of this component (xm_k, ym_k) is taken as the measurement (z_k) at frame k and is used to predict the position of the cell in frame $(k+1)$.

3. EXPERIMENTAL RESULTS

Satellite cells are activated 24 hours prior to imaging through the process of producing myofiber explants by dissecting muscle from the hind limbs of female mice and culturing 3 to 5 myofibers per well containing collagen and growth serum [4]. There were about 65 experiments (on 48-well plates) with 20 to 30 fields imaged at $10\times$ with a sampling interval of 10 minutes over 24 hours to yield a set of 122 movies (145 frames each) for 250 control cells that satisfied the viability and visibility criteria. We applied the proposed technique to five satellite cell sequences (556 frames and 6 cells) with associated ground truth provided by a biologist expert. Each frame is 16-bit gray scale of spatial size 1344×1024 pixels and resolution of 0.6143 μm per pixel.

Since no benchmark exists for this particular problem, we evaluate the successive improvements in tracking resulting from each additional step compared to manual tracking. Using only the particle filter (PF), the measurement is obtained directly from I_k, as discussed in Section 2.3. The second method RPF applies illumination correction and registration followed by PF-based tracking. The third method RBPF applies all three steps including background removal. Using domain knowledge, we set R=C=20 pixels. For computing the background, we experimentally chose a window size of w=11. The process noise u_t and measurement noise v_t are normally distributed. Since each satellite cell shows different dynamic behavior, the parameters of the state transition function f_s and measurement function f_z are adapted for each cell and chosen experimentally. We have employed 10,000 particles to estimate the position of the centroid in each frame. A large number of particles were required for high accuracy.

Performance advantage of RBPF is measured using tracking (distance) error, and recall (with restarts). The distance error, E_{kqm}, in frame k for cell object q and method $m = \{\mathrm{PF}, \mathrm{RPF}, \mathrm{RBPF}\}$ is given by:

$$E^2_{kqm} = (x_{kq,\mathrm{GT}} - x_{kqm})^2 + (y_{kq,\mathrm{GT}} - y_{kqm})^2 \qquad (7)$$

where,$(x_{kq,\mathrm{GT}}, y_{kq,\mathrm{GT}})$ is the ground truth for cell q in frame k and (x_{kqm}, y_{kqm}) is the estimated cell position for cell q in frame k obtained by method m. The average distance tracking error for a particular sequence is given by the mean and standard deviation, $\mu_E \pm \sigma_E$, of E_{kqm} for all cells across all frames (excluding occluded or large motion frames). Since the proposed method is semi-automated, we also report the total number of restarts (for all cells) and percent recall performance over all cells in each sequence.

Table 1. Tracking performance of PF, RPF and RBPF methods for five sequences showing number of ground truth frames (GF), number of cells tracked in that sequence (C), number of prespecified restarts (R), recall accuracy in percent with restarts, average distance error.

S	GF	C	R	Recall (%)			$\mu_E \pm \sigma_E$ of E_{kqm} (μm)		
				PF	RPF	RBPF	PF	RPF	RBPF
1	181	2	8	38	53	85	38.6±22.9	16.7±11.7	2.3±1.7
2	128	1	4	42	61	85	27.4±13.6	11.4± 9.2	2.1±1.1
3	90	1	4	36	49	93	40.4±16.2	17.4±12.5	3.1±2.1
4	73	1	3	44	65	91	25.2±12.6	10.4± 9.1	2.1±0.9
5	84	1	5	31	48	60	33.4±18.7	17.5±11.3	2.4±1.6
Average				38	55	83	33.0±16.8	14.7±10.8	2.4±1.5

Given the ground-truth (GT) for all cells in a sequence, the number of restarts is fixed and is the same for all three methods. A track is restarted after an occlusion or when there is more than a 90° directional change in cell motion between adjacent frames. Note that these *skipped frames* are not included in the distance error metric. We use a bounding box (whose dimension is about the average cell size) with its center based on the algorithm estimated centroid. The recall for a sequence is defined as the ratio of number of frames where GT-BBox and Algorithm-BBox overlap by at least 50%, divided by the GT length for all cells. Note that with manual restarts, recall is a more suitable measure.

Table 1 shows that each of the three steps in the proposed approach is important. Average improvement in tracking error of RPF over PF is 56% and that of RBPF over RPF is 83%. Average recall of RPF is 45% higher than PF and average recall of RBPF is 51% higher than RPF. The superiority of RBPF over RPF and PF is further qualitatively illustrated in Fig. 2, which shows the tracking results for two cells over five different frames from Sequence 1. The ground truth (cell centroids) are shown as red circles. In PF, stage motion is not corrected, so predictions drift. The measurements for PF are taken from the actual unregistered images where the effects of poor illumination and contrast are also present leading to large tracking errors. In RPF, although we correct for stage motion and illumination variation, no background removal is applied resulting in many false alarms and erroneous measurements. In RBPF, we reduce the error due to stage motion and also correct for illumination variation. Then using background modeling and subtraction we obtain a more accurate set of cell detections, for which PF provides better predictions and tracking accuracy. The average execution time of RBPF is 7.1 seconds per frame on a standard PC (Intel core i5, 6GB).

4. CONCLUSIONS AND FUTURE WORK

In this paper, we propose a systematic algorithm to track satellite cells moving on the 3D surface of myofibers in timelapse brightfield video microscopy. This problem is challenging due to satellite cells moving out of the focal plane which makes them difficult to detect, frame to frame jitter from stage motion and other factors. In the first step, we perform im-

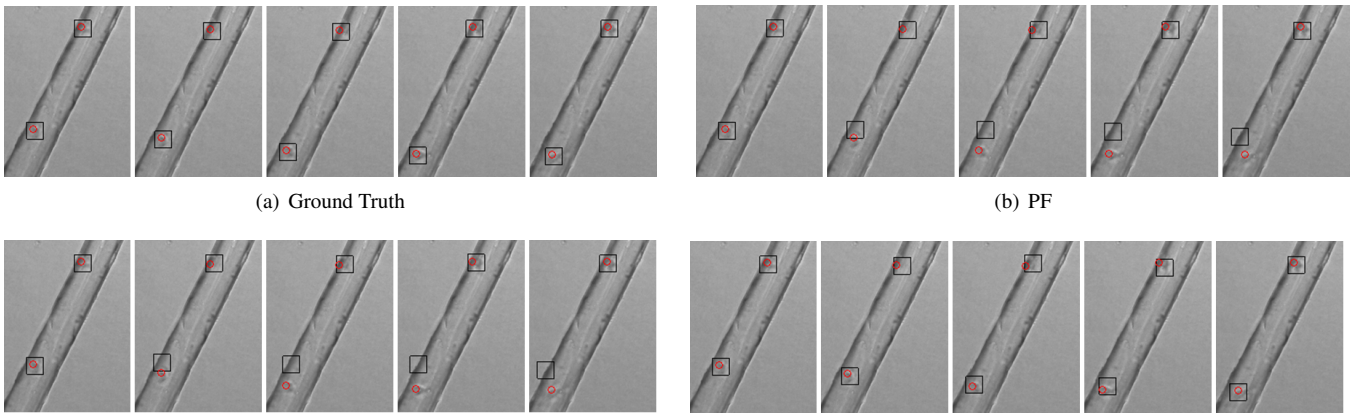

(a) Ground Truth (b) PF

(c) RPF (d) RBPF

Fig. 2. Results of tracking two satellite cells over 5 frames (005-009) in Seq. 1 with center of bounding boxes being estimated cell centroids.

age registration to correct for jitter and illumination variation. Next, we model the background by estimating local medians over a group of frames and subtracting this background model from the registered image to obtain robust cell movement detections. Finally, particle filter-based tracking is used to predict and associate the position of the cells using the detections. In the future, we plan to handle problems with out of plane motion and abrupt changes in cell movement direction, stationary cells [18], dividing cells and to eliminate the need for manual restarts [19], as well as speed up the algorithm.

5. REFERENCES

[1] T.J. Hawke and D.J. Garry, "Myogenic satellite cells: physiology to molecular biology," *J. Applied Physiology*, vol. 91, no. 2, pp. 534–551, 2001.

[2] X. Shi and D.J. Garry, "Muscle stem cells in development, regeneration, and disease," *Genes & Development*, vol. 20, no. 13, pp. 1692–1708, 2006.

[3] R. Bischoff, "Regeneration of single skeletal muscle fibers in vitro," *Anatomical Record*, vol. 182, no. 2, pp. 215–235, 1975.

[4] A.L. Siegel, K. Atchison, K.E. Fisher, G.E. Davis, and D.D.W. Cornelison, "3D timelapse analysis of muscle satellite cell motility," *Stem Cells*, vol. 27, no. 10, pp. 2527–2538, 2009.

[5] N. Ray, G. Dong, and S.T. Acton, "Tracking multiple cells by correspondence resolution in a sequential bayesian framework," in *IEEE ICIP*, 2005, vol. 1, pp. 705–708.

[6] K. Li, E.D. Miller, M. Chen, T. Kanade, L.E. Weiss, and P.G. Campbell, "Cell population tracking and lineage construction with spatiotemporal context," *Medical Image Analysis*, vol. 12, no. 5, pp. 546–566, 2008.

[7] S. Nath, K. Palaniappan, and F. Bunyak, "Cell segmentation using coupled level sets and graph-vertex coloring," *Lecture Notes in Comp Sci (MICCAI)*, vol. 4190, pp. 101–108, 2006.

[8] A. Mosig, S. Jaeger, W. Chaofeng, S. Nath, I. Ersoy, K. Palaniappan, and S.S Chen, "Tracking cells in live cell imaging videos using topological alignments," *Algorithms for Molecular Biology*, vol. 4, pp. 1–9, 2009.

[9] A.S. Chowdhury, R. Chatterjee, M. Ghosh, and N. Ray, "Cell tracking in video microscopy using bipartite graph matching," in *IEEE Int. Conf. Pattern Recognition*, 2010, pp. 2456–2459.

[10] F. Bunyak, K. Palaniappan, S.K. Nath, T.I. Baskin, and G. Dong, "Quantitative cell motility for *in vitro* wound healing using level set-based active contour tracking," in *Proc. IEEE Int. Symp. Biomedical Imaging (ISBI)*, 2006, pp. 1040–1043.

[11] A.S. Chowdhury, R. Roy, S. Bose, F. Khalifa, A. Elnakib, and A. El-Baz, "Non-rigid biomedical image registration using graph cuts with a novel data term," in *Proc. IEEE Int'l Symp. Biomedical Imaging*, 2012, pp. 1–4.

[12] B. Zitova and J. Flusser, "Image registration methods: A survey," *Image and Vision Computing*, vol. 21, no. 11, pp. 977–1000, 2003.

[13] K. Palaniappan and *et al.*, "Efficient feature extraction and likelihood fusion for vehicle tracking in low frame rate airborne video," in *13th Conf. Information Fusion*, 2010, pp. 1–8.

[14] M.S. Arulampalam, S. Maskell, N. Gordon, and T. Clapp, "A tutorial on particle filters for online nonlinear/non-Gaussian Bayesian tracking," *IEEE Trans. Signal Proc.*, vol. 50, no. 2, pp. 174–188, 2002.

[15] M. West and J. Harrison, *Bayesian forecasting and dynamic models*, Springer. Springer Verlag, 1997.

[16] J. Olsson, O. Cappé, R. Douc, and E. Moulines, "Sequential monte carlo smoothing with application to parameter estimation in nonlinear state space models," *Bernoulli*, vol. 14, no. 1, pp. 155–179, 2008.

[17] G. Kitagawa, "Monte carlo filter and smoother for non-gaussian nonlinear state space models," *Journal of Computational and Graphical Statistics*, pp. 1–25, 1996.

[18] I. Ersoy and K. Palaniappan, "Multi-feature contour evolution for automatic live cell segmentation in time lapse imagery," in *30th Int. IEEE Engineering in Medicine and Biology Society Conf. (EMBC)*, 2008, pp. 371–374.

[19] B. Han, Y. Zhu, D. Comaniciu, and L. Davis, "Kernel-based Bayesian filtering for object tracking," in *IEEE Conf. Computer Vision Pattern Recognition*, 2005, vol. 1, pp. 227–234.